University of Thi-Qar Journal for Engineering Sciences
Volume 16, Issue 1, June 2026
https://doi.org/10.32792/utq/utjes.16.1.737

Simulating SPWM Effects of Switching Frequency, Modulation Index, and Load types on Induction Motor Performance

Mohammed R Brayyich*[1]

Received:18th December 2025/Accepted: 3rd February 2026/ Published Online: 1st June 2026

Abstract

Understanding the factors that affect induction motor performance is key to improving energy efficiency and reliability in industrial use. This study examines how switching frequency, modulation index, and load types (fan, pump, and standard) influence motor performance. We applied sinusoidal pulse width modulation to control the DC-AC converter in MATLAB/Simulink. Fan and pump loads follow torque that rises with the square of speed. They bring special challenges unlike standard loads. These include higher aerodynamic, hydraulic, and friction losses. Results show that switching frequencies above 1 kHz enhance voltage waveforms. They lead to peak motor efficiency of 80% and cut total harmonic distortion to 21%. Modulation indices affect performance in both linear and non-linear ways. Efficiency rises steadily to 77% as the index reaches 0.8. Voltage also grows consistently in under and over modulation regions. Yet current, input power, speed, and harmonic distortion vary non-linearly during overmodulation. The lowest total harmonic distortion occurs at index 1. Fan loads show slightly higher losses, up 7.34%, and lower efficiency, down 1.57%, compared to standard loads. Pump loads, however, feature much lower losses, down 37%, alongside reduced efficiency of 5.8%.

Keywords **—** Switching frequency, Modulation index, Total harmonic distortion, Motor efficiency, Sinusoidal pulse width modulation, Frequency ratio**.**

1 Introduction

Three-phase induction motors (IMs) hold great importance in industrial factories. They are straightforward to run and demand minimal maintenance. Moreover, they offer excellent flexibility for frequency adjustments. This enables control over speed, power draw, and voltage levels. These qualities make them essential in harsh settings like mines and chemical plants. With the advancements in electronic technology, there is a strong focus on improving energy efficiency and reducing vibrations of these motors, with a focus on their switching frequency (f_c) using Pulse Width Modulation (PWM). PWM allows for manipulation of the output voltage by changing the input voltage or adjusting the boost that the inverter provides. The discussion of PWM and its role in improving motor performance is highly relevant to both industrial.

Krings et al. have studied the affection of modulation index and switching frequency on permanent magnet synchronous machine (PMSM) (Krings et al., 2013). The switching frequency range between 1kHz and 20 kHz and the modulation index between 0.2 and 0.9. the results shows that the switching nature process of the PWM makes the iron losses increased by 30%. While, the high switching frequency and modulation index make the iron losses unsignificant. Asker et al. investigate and simulate the voltage, current and harmonic of the PWM output (Asker & Kilic, 2017). The inverter supplied a RL three phase load. The investigation switching frequency range is between 450 Hz and 17000 Hz and modulation index in three steps 0.3, 0.8 and 2. The results show that the increasing the switching frequency decrease the low order harmonics. At low modulation indices, the main

Mohammed R Brayyich
m.r.brayyich@utq.edu.iq
1 Department of Electrical and Electronics Engineering, University of Thi-Qar, Nasiriah,64001, Thi-Qar, Iraq

harmonic dominates with minimal side bands. In over-modulation, the inverter produces more significant harmonics, resembling square wave operation. Raghuwanshi et al. have analysis the affection of modulation index and frequency index on 3-ph induction motor (Raghuwanshi et al., 2017). The simulation done on the motor controlled by PWM with inverter with modulation index Range between 0.7 and 0.99 and frequency index BETWEEN 500 and 750 Hz. The results show that as the modulation reaches one so the total harmonic distortion (THD) decrease in voltage and current. And, increasing the modulation frequency let to drop in the THD of the voltage and current, line voltage rotor speed. Jung et al. have studied the current ripple of motor fed by PWM inverter (Jung et al., 2018). The results show the 51% reduction in switching frequency at 1.12 modulation index. Solangi et al. have studied the modulation index affection on the harmonic of single phase universal motor fed by PWM inverter (Solangi et al., 2018). In their paper, the modulation index parameter is used to analyze current's THD. the result shows that the higher modulation (less than one) index the less harmonic content. Al-Adwan et al. have analysis the modulation index and the carrier frequency effect on the total harmonic distortion of the single phase PWM inverter's output (Al-Adwan & Al Shiboul, 2020). Simulation ranges of the modulation index and carrier frequency are 0-1 and 100-200 Hz. The results shows that the increasing the carrier frequency let to reduction in lower harmonics. Moreover, the higher modulation index, the lower total harmonic distortion. Sharms et al. have investigate the modulation index effect on a motor fed by space vector PWM inverter (Sharma et al., 2020). The simulation conducted in MATLAB/Simulink. The modulation index range limited between 0.6 and 1.5. the results show that the voltage reaches it maximum when modulation index reaches unity, and then falls again when modulation index below unity. Also, proved that the motor speed depends on modulation index. Sarigiannidis et al. have investigate the relationship between torque ripple and harmonic loses, with Switching frequency of a surface permanent magnet motor. The simulation and testing measurements shows that the ripple torque and THD decreased with the increase of switching frequency (Sarigiannidis & Kladas, 2015). Busacca et al. have investing the impact of switching frequency on efficiency and THD. LabVIEW simulation next to Laboratory testing have been conducted for three-phase five-level power inverter. The results shows as switching frequency improve the efficiency also increased, and the THD decreased (Busacca et al., 2022). This research for improve the inverter performance without a motor. Diyoke et al. have presented the relationship between the modulation index and induction motor supplied by multilevel inverter (Diyoke et al., 2024). The simulation conducted in MATLAB/Simulink considering the modulation index is 0.7-1.2 for fixed load torque values. The results shows that the motor speed and steady state time at 2 N load, increases as the m_i increased. While at 4 N load the behaviors of the relation becomes nonlinear. This research focused on multi-level of fixed torque only. On the other hands some papers studies control methods to optimize the waveform method using PID and sliding mode learning techniques (Mohammed & Hadi, 2024). Overall view of this literature comparison has been shown in

Ref	**Switching Frequency**	**Modulation index**	**Load Type**
(Krings et al., 2013)	(1-20) kHz	0.2-0.9	Regular load
(Asker & Kilic, 2017)	(0.45-17) kHz	0.3, 0.8, 2	Regular load
(Raghuwanshi et al., 2017)	(500-750) Hz	0.7-0.99	Regular load
(Jung et al., 2018)	variable	Variable	Regular load
(Solangi et al., 2018)	Fixed	Variable	Regular load
(Al-Adwan & Al Shiboul, 2020)	(100-200) Hz	0-1	No motor
(Sharma et al., 2020)	Fixed	0.6-1.5	Regular load
(Busacca et al., 2022)	10-70 KHz	0.3-1.15	No motor
(Diyoke et al., 2024)	Fixed	0.7-1.1	Regular load
This research	50-5 kHz	0.2-2	Fan/Pump/Regular Load

Table 1. Furthermore, the switching frequency and modulation index should be tested for wide range to fully understand the performance of a motor.

Ref	**Switching Frequency**	**Modulation index**	**Load Type**

(Krings et al., 2013)	(1-20) kHz	0.2-0.9	Regular load
(Asker & Kilic, 2017)	(0.45-17) kHz	0.3, 0.8, 2	Regular load
(Raghuwanshi et al., 2017)	(500-750) Hz	0.7-0.99	Regular load
(Jung et al., 2018)	variable	Variable	Regular load
(Solangi et al., 2018)	Fixed	Variable	Regular load
(Al-Adwan & Al Shiboul, 2020)	(100-200) Hz	0-1	No motor
(Sharma et al., 2020)	Fixed	0.6-1.5	Regular load
(Busacca et al., 2022)	10-70 KHz	0.3-1.15	No motor
(Diyoke et al., 2024)	Fixed	0.7-1.1	Regular load
This research	50-5 kHz	0.2-2	Fan/Pump/Regular Load

Table 1: Comparison of previous works

SPWM inverters are one of the most dynamic kinds of inverters and play a major role in motor operation control. This study proposes a simulation model of fan induction motor (FIM) control utilizing MATLAB/Simulink software and Sinusoidal Pulse Width Modulation (SPWM) inverters. This research's contributions are:

- Analyzing f_c effect on the performance of FIMs, ranging from 50 Hz to 5 kHz which is lower and higher than Ref. (Raghuwanshi et al., 2017) and Ref. (Sharma et al., 2020) respectively.
- Examines the m_i impact on the FIM performance. m_i rang is 0.2-2 which is beyond the Ref. (Asker & Kilic, 2017) and Ref. (Sharma et al., 2020) ranges respectively.
- Investigate the variation in motor performance with different load types (regular, fan, pump), rather than just regular loads as in Ref. (Raghuwanshi et al., 2017), (Jung et al., 2018), (Sharma et al., 2020), (Busacca et al., 2022), (Diyoke et al., 2024).

The rest of the paper is organized as follows, section II methodology, section III simulation and results discusses, section IV conclusion.

2 Methodology

2.1 Speed Control of Induction Motors

Before the advent of modern solid-state controllers, IMs were generally not considered suitable for applications where speed needed to be controlled over a wide range. The normal operating range of an IM is limited to a slip of less than 5%, and speed changes within this range are more or less linearly proportional to the load on the motor. Even if slip can be increased, motor efficiency decreases significantly because rotor copper losses (P_{RCL}) are directly proportional to slip (s) as shown in Eq. **Error! Reference source not found.** (Klimenta et al., 2018).

$$P_{RCL} = s \cdot P_{AG} \quad (1)$$

Where, P_{AG} denotes the air-gap power, which is the power transferred across the air gap from the stator to the rotor. In fact, there are only two methods for controlling the speed of IMs. One method is to change the synchronous speed, meaning the speed of the magnetic fields of the rotor and stator, as the rotor speed always remains close to synchronous speed. The other method is to control the slip for a given load (Marino et al., 2010).

The popular method is the voltage/frequency method. In this method, if the voltage-to-frequency ratio is kept constant, flux remains constant as well. Maximum torque, which is independent of frequency, can be maintained almost constant. However, at low frequencies, the air gap decreases due to the reduction in stator impedance, and therefore, the voltage must be increased to maintain the torque constant. This control method is commonly referred to as volts per hertz control (Amin, 2001). As frequency decreases, the slip and the change in maximum torque increase. Speed can be controlled for a specific torque by changing the frequency; therefore, torque and speed can be controlled by varying voltage and frequency. Usually, torque is kept constant while speed is varied (Rahman et al., 2019).

2.2 PWM Inverter

Figure 1-(a) illustrates a general schematic of a PWM inverter. In PWM inverters, the output AC voltage can be controlled. Therefore, it can be supplied with a constant DC voltage. When the input source is of the DC type, the first design scheme is utilized. When the voltage source is of the AC type, the inverter employs a diode bridge, as depicted in the Figure 1-(b). There are various methods to generate pulse width modulation, with one of the most important ones being SPWM. Additionally, other types have been used in other applications, such as space vector pulse width modulation (SVPWM)(Ali et al., 2016; Hassain et al., 2018).

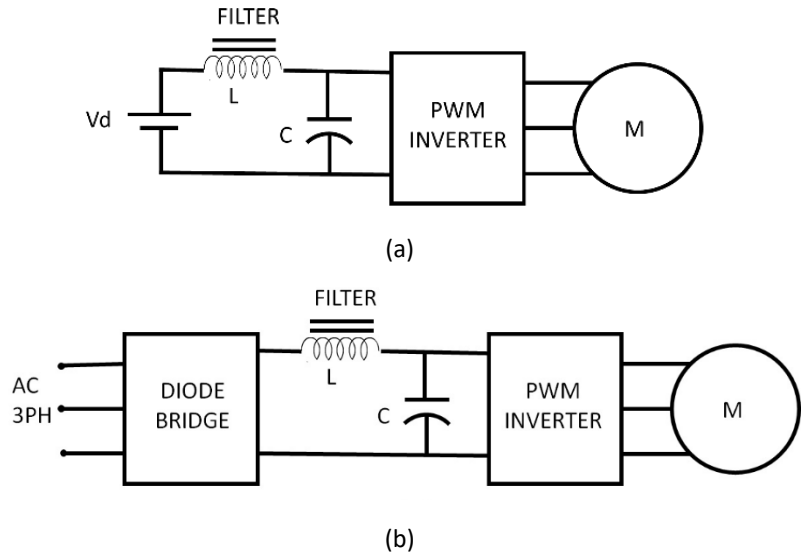

Figure 1: General diagram of a PWM inverter (a) Inverter with DC input (b) Three-phase inverter with AC input

2.3 Sinusoidal Pulse Width Modulation

In this method, three reference voltages V_{ra}, V_{rb}, and V_{rc} with a variable amplitude A are compared in three comparators to a triangular carrier wave V_{CW} with an amplitude B, as shown in Figure 2.

The outputs of the comparators and the Not blocks 1, 3, 5 and 4, 6, 2 are control gate signals (G) applied to the three phases of the inverter, formed by pairs of switches (s1, s4), (s3, s6), and (s5, s2), respectively. Consider the pair of switches (s1, s4). These switches gate control (G1, G4) the phase A voltage of the motor. The phase A voltage relative to the midpoint of the DC supply (O) is determined. According to Figure 3, the reference wave V_{ra} is compared to the carrier voltage V_{CW} in comparator. When voltage A is greater than voltage B, the signal is applied to switch S1 gate (G1). Conversely, when voltage A is less than voltage B, it is applied to switch S4s gate (G4) using a NOT block as shown in Figure 2.

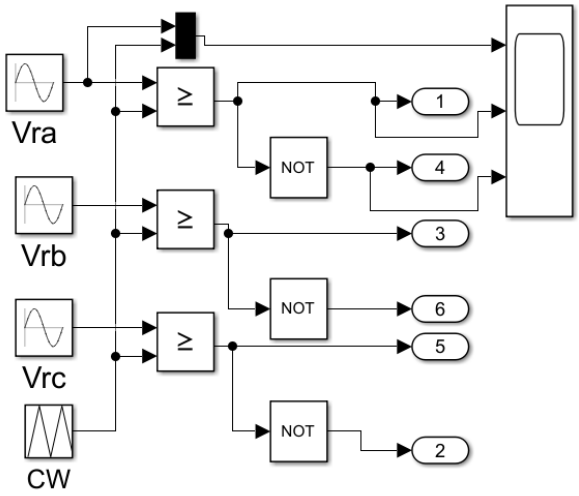

Figure 2: SPWM pulse generator Block diagram

The waveforms in Figure 3 are plotted for a single cycle of the reference waveform, corresponding to twenty cycles of the triangular waveform. Similarly, G_3 and G_5 voltages can be obtained by considering the phase shifting G1 by $2 * \frac{\pi}{3}$ and $4 * \frac{\pi}{3}$, and status of the pairs of switches (S_3, S_6) and (S_5, S_2), respectively. This method is called SPWM.

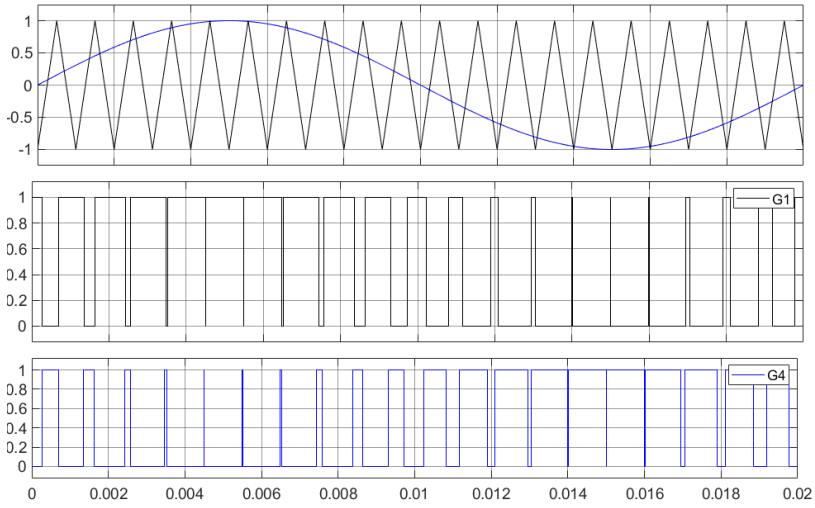

Figure 3: The switches gate control G1 and G2 generated by SPWM

The resulting waveforms (V_{ab}) for the period is shown in Figure 4.The line voltage V_{AB} is obtained by subtracting V_{BO} from V_{AO}. Similarly, V_{BC} and V_{CA} can also be obtained.

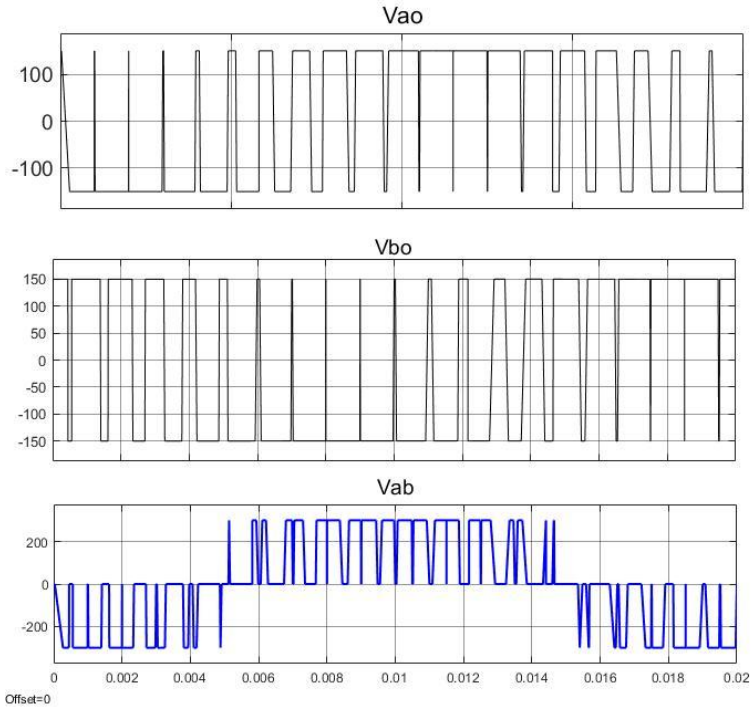

Figure 4: The inverter Output voltages Vao and Vbo and Vab

It is noteworthy that the fundamental frequency of the motor voltage is similar to the frequency of the reference sinusoidal voltages (f). Therefore, the motor voltage frequency changes with the reference voltage frequency. The ratio of the reference wave amplitude A_r to the carrier wave (A_c) with mi denotes modulation index, as shown in Eq.(1).

$$mi = \frac{A_r}{A_c} \tag{1}$$

The effective value of the primary component in the waveform $\mathrm{V_{ao}}$ can be determined by Eq.(2). Here, Vdc denotes the amplitude of the input DC voltage. Consequently, an increase in mi leads to a linear rise in the effective value of the primary component.

$$V_{ao}^{rms} = \frac{m\,.\,V_{dc}}{2\sqrt{2}} \tag{2}$$

The waveform V_{ao} incorporates odd multiple harmonics of the fundamental frequency, while harmonics that are even multiples are negligible. Eq.(3) introduce a frequency ration parameter P.

$$P = \frac{f_c}{f} \tag{3}$$

Here, f_c stands for the carrier wave frequency, and f represents the reference wave frequency. A large value of P indicates that the frequency of harmonics is substantial compared to the primary component. The nominal value of machine leakage inductance serves to filter out these harmonics. Hence, power transistors are preferred for low-power applications, while GTOs and IBGT are favored for medium-power applications. In comparison to SPWM, uniform sampling modulation exhibits smaller low-frequency harmonic components.

2.4 Induction motor and loads Modulation

Fan loads are commonly encountered in industrial applications, such as cooling systems, ventilation, and HVAC

. These applications require careful consideration of fan and pump loads in PWM inverter-fed induction motors. These loads have varying torque requirements. Their torque depends on environmental conditions. Temperature and Humidity affect their torque demand. PWM inverters enable precise control of the induction motor's speed. This allows the system to adapt efficiently to load variations. As a result, the overall performance and reliability improve. The motor load is modeled as a fan, where mechanical torque (T_m) varies proportionally with the square of speed(W_m) as shown in Eq. (4) (Asif et al., 2016; Rachev & Dimitrov, 2022).

$$T_m = 0.0004 * W_m^2 \quad (4)$$

Where W_m is the motor speed. IMs can sustain serious damage when they stall in fan applications because of inadequate torque (Thomson & Culbert, 2016). By dynamically regulating the motor speed to prevent stalling, PWM inverters reduce this danger and provide safe, continuous operation (Nandi et al., 2005). Furthermore, significant energy savings can result from optimizing fan speed using PWM control, particularly during times of low load demand. This ability to tailor the induction motor's performance to real-time requirements results in both operational efficiency and reduced energy consumption (Al-Adwan & Al Shiboul, 2020). However, there are another type of loads with a constant torque value in the industry regularly (Birowo et al., 2015). The FIM is configured with a power rating of 1.5 kW. Additional parameters are detailed in Table 2.

Table 2: Parameters of the Tested 3-Phase Induction Motor (1.5 kW)

Voltage	**220V**	**Frequency**	**50 Hz**
Speed	1433 rpm	Poles	2
Stator Resistance (Rs)	0.8889 Ω	Stator Leakage Inductance (Lls):	0.003727 H
Rotor Resistance (Rr)	1.3479 Ω	Rotor Leakage Inductance (Llr):	0.005098 H
Magnetizing Inductance (Lm)	0.09441 H	Inertia (J):	0.005398 kg-m²

In addition, Pump loads, like centrifugal pumps, have torque proportional to the square of speed, described in Eq. (6)-(8) (Guo et al., 2017).

$$\frac{P}{P_o} = \frac{n^3}{n_o^3} \quad (5)$$

$$T_L = P/n \quad (6)$$

$$T_L = \frac{P\_o}{n\_o\text{^}3} \; . \; n\text{^}2 \quad (7)$$

Where, n_o, n are rated speed and speed of the pump, P_o, P are the rated power and shaft power of the pump. Eq. (8) is quadratic relationship arises because as speed increases, flow increases linearly, head increases with speed squared, and power (and torque) scale accordingly, which is resulting from inserting Eq. (6) in Eq. (7), pump parameters shown in Table 3.

Table 3: Parameters of the centrifugal pump

$\boldsymbol{n_o(rpm)}$	$\boldsymbol{P_o(kw)}$
2433	1.5

3 Simulation and Results Discussion

The simulation depicted in Figure 5 showcases the open-loop control of an FIM using PWM modulation. The parameters configured for the squalor-cage rotor motor entail two pairs of poles, a power rating of 2 hp, a voltage of 220 V, and a frequency of 50 Hz, more parameters shown previously in Table 2. The IGBT parameters based on IKP40N65F5 IGBT model from Infineon (Infineon Technologies AG, 2013). Given that the output frequency of the inverter aligns with the reference waveform frequency, we establish the reference waveform frequency as 50 Hertz.

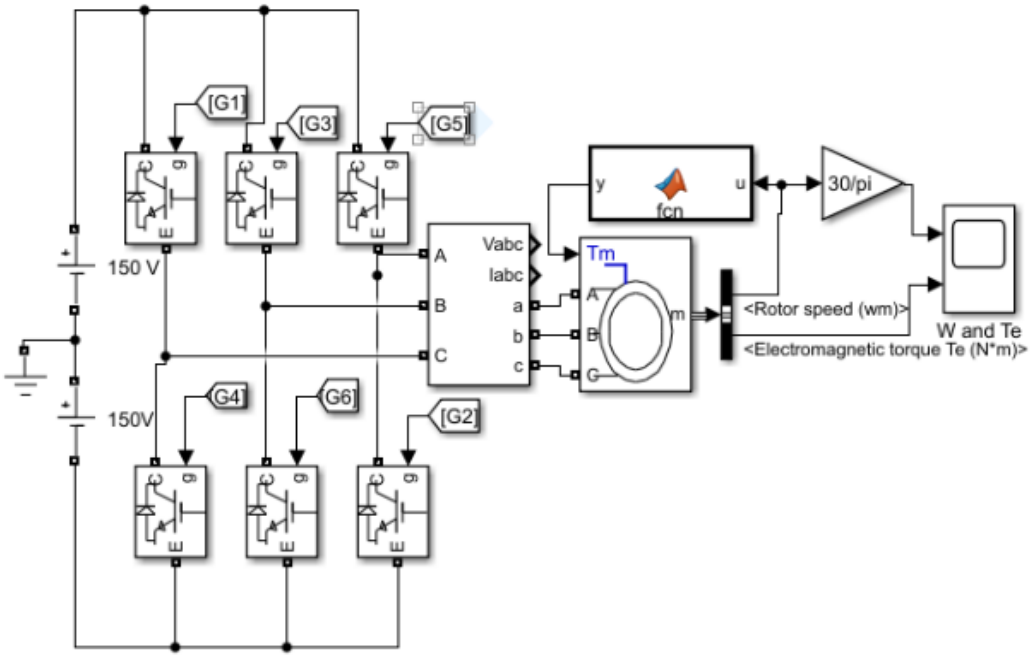

Figure 5: Inverter and Induction motor Simulation in Simulink MATLAB

The objective of this simulation is threefold: first, to examine the waveform of the voltage and current output of the inverter (equivalent to the input voltage and current of the IM), and second, to explore the impact of PWM f_c arising from changes P parameter on the voltage and current harmonics of the FIM. Additionally, explore the impact of m on the FIM performance. Lastly, motor performance comparison for regular vs fand vs pump loads. The comparison based on two types of parameters. First, inverter parameters which are voltage, current and total harmonic distortion (THD) where fast Fourier transform analyzer (FFT) app have been used in MATLAB (*FFT Analyzer*, n.d.). Second, motor performance which are the shift speed, input/output power, power losses and efficiency as shown in Eq. (9)-(12).

$$p_{in} = Va\,.Ia + Vb\,.Ib + Vc\,.Ic \quad (8)$$

$$p_{out} = T_e * W_m \quad (9)$$

$$p_l = p_{in} - p_{out} \quad (10)$$

$$\lambda = \frac{p_{out}}{p_{in}} \quad (11)$$

Where, $p_{in}, p_{out}, p_l, \lambda, T_e$ are the input power, output power, power losses, motor efficiency and electrical torque respectively.

3.1 Impact of P variation on motor performance

The variation of P, defined as shown in Eq. (3), where f is the motor frequency (50 Hz), has a significant impact on the performance of IMs. This section explores the relationship between P and key performance metrics, including stator voltage (V_a), stator current (I_a), input power (P_{in}), speed (N), and Total Harmonic Distortion of stator current (THD(Ia)), and waveforms with insights derived from the experimental results. Initially, we set the carrier wave frequency to 50 Hz, as shown in Figure 6. A low PWM carrier frequency f_c significantly increases harmonics in the motor's voltage and current, which weakens the waveforms. This leads to high-speed ripples and strong torque pulsations until the motor reaches its rated speed.

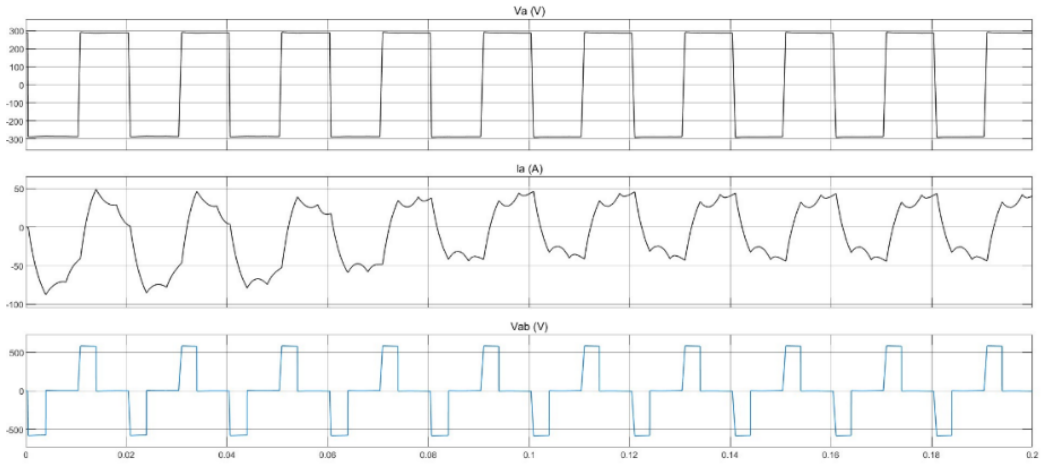

(a)

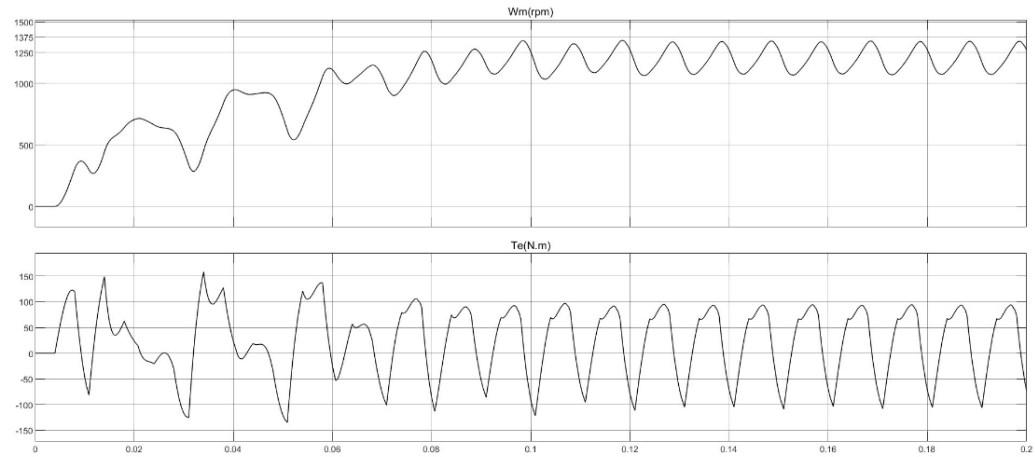

(b)

Figure 6: Motor performance results when fc = 50 Hz (a) Voltage and Current waveform (b) Speed and Torque diagram

Next, we set the carrier wave frequency to 1 kHz ($p = 20$). Higher f_c smooths voltage and current waveforms, as shown in Figure 7. Because harmonics drop sharply. Thus, motor performance improves, with speed stabilizing under steady-state conditions. Additionally, the torque pulsations decreasing noticeably.

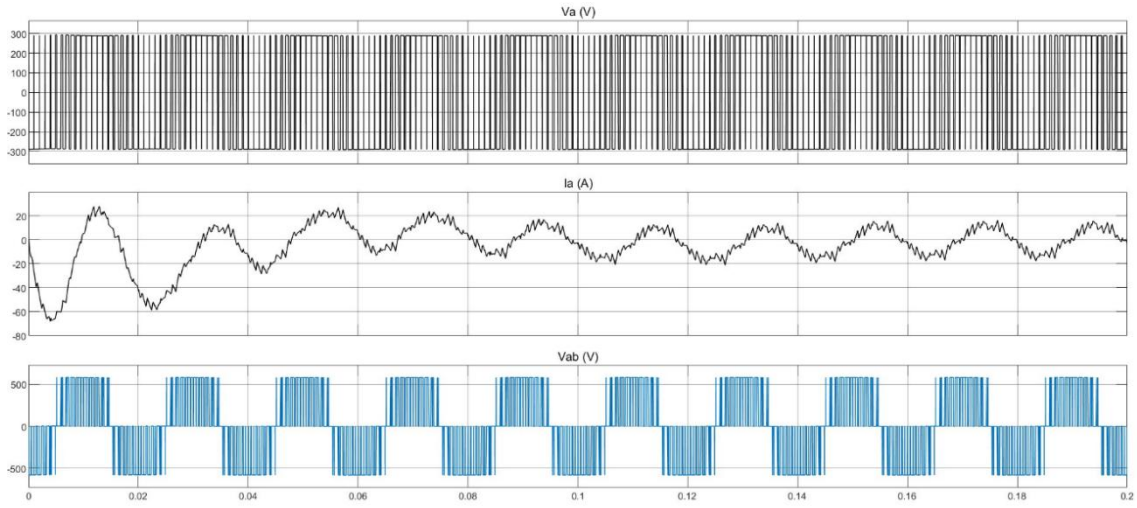

(a)

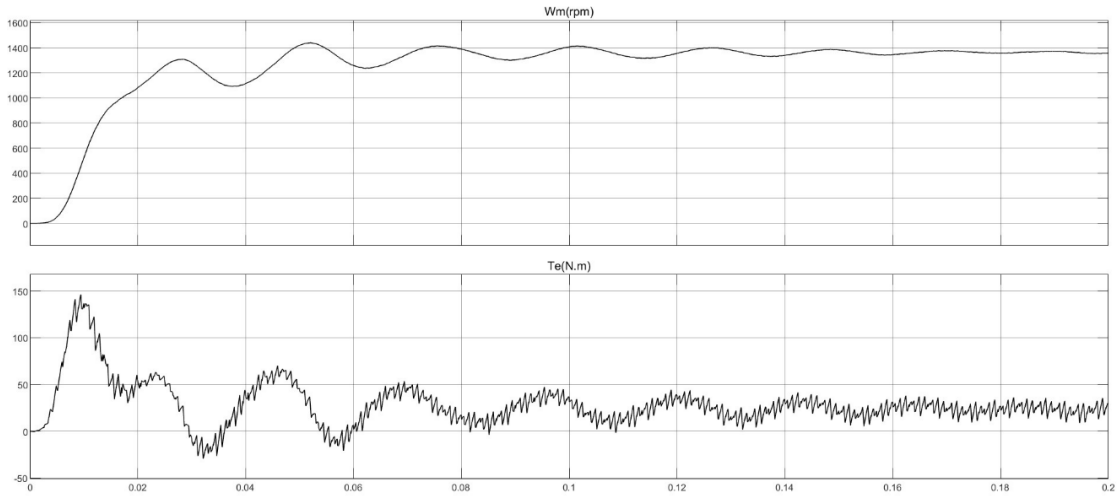

(b)

Figure 7: The results when fc= 1000 Hz (a) Voltage and Current waveform (b) Speed and Torque diagram

Table 4 shows how changes in p affect fan induction motor performance. Voltage V_a drops slightly. It moves from 259 V at p=1 to about 205 V for $p \geq 20p$. Current I_a drops from 29.9 A at p=1 to roughly 9 A for p≥20. Thus, higher switching frequencies cut voltage stress and input energy.

Table 4: Impact of P Variation on Fan Induction Motor Performance

P	fc (Hz)	Va (V)	Ia (A)	P_{in} (W)	N (rpm)	P_{out} (W)	λ (%)	Losses (W)	THD%(Ia)
1	50	259	29.9	10670	1272	2216	20	6449	32
2	100	241	24.4	10050	309	37.14	0.36	10045	41
3	150	240	10.9	1447	1275	3067	55	2424	42
10	500	209	9.86	4147	1341	3172	76	974	59
15	750	204	8.9	4364	1317	3104	71	1260	32
20	1000	205	9	3986	1359	3197	79.8	789	21
30	1500	207	9	3977	1370	3176	79.8	800	11
100	5000	205	9.2	3976	1365	3177	80	799	3

At lower p, the motor needs higher input power. For example, 10670 W at $p = 1$. Due to high THD (32%), which distorts the waveform. The distorted current waveform causes high copper losses. As p increases, P_in stabilizes around 3976 W for p ≥ 20. This shows more efficient power use. The output power (Pout) and the motor's speed (N) fluctuate at first. It then steadies at p ≥ 20 about 3176–3197 W and for 1365–1370 rpm, respectively. This indicates reliable load handling and consistent mechanical performance. Efficiency (λ) improves greatly with p. At p = 1, it is only 20% due to high THD in the current. This distorts the waveform, raises current levels, and adds copper and core losses (Lai & Chen, 2001). However, λ rises steadily to 80% at p = 100. Losses drop from 6449 W at p = 1 to 799 W at p = 100, which highlights better energy use. THD(Ia), falls as p rises. At lower p, it reaches 32% at $p = 1$. This signals major waveform distortion. As p grows to 100, THD(I_a) drops to 3%. This reflects cleaner current waveforms and less harmonic interference.

Motor losses tend to be the same as the efficiency. At lower p, the motor has high losses due to high harmonic distortion. It leads to poor waveform quality and efficiency. As p increases to $p = 30$, the motor achieves more stable operation, with reduced losses and better waveform. The motor reaches peak efficiency, minimal losses, and very low $THD(I_a)$ at $p = 100$.

In conclusion, these results highlight the important relationship between p and motor performance indices.

Higher p values, improve efficiency, reduce losses, and enhance waveform quality (Lai & Chen, 2001; Nasir, 2022). The relationship in this context is not linear, unlike the previous studies (Almani et al., 2021)(Dems & Komeza, 2022).

3.2 Impact of Modulation index on motor performance

Using a 500 Hz f_c, the effect of the modulation index on motor performance was investigated.

shows that when m_i exceed 0.8, nonlinearity performance surfaces. For instance, at m_i = 1.2. Despite an increase in input power to 8,261 W, the speed decreases to 1,069 rpm, and efficiency to 31.3%, while THD remains high at 29.3%. This high THD leads to distortion effects, disrupting torque generation and electromagnetic stability. At $m\_i = 1.8$ and 2, THD further escalates beyond 57%. However, output power varies between 3,300 W and 3,570 W, and efficiency varies between 60 and 78%, which are signs of harmonic-induced torque ripple changes. These results confirm the drawback of overmodulation in SPWM , leading to waveform clipping and harmonics that reduce efficiency (IbraheemAbood & Sabri A. Raheem, 2014; Raghuwanshi et al., 2017). This nonlinear behavior stems from SPWM's inherent limitation. The linear modulation index maxes out near 0.785 (π/4). Beyond this, voltage waveforms clip and generate substantial harmonics. The distorted waveform increases copper and iron losses in the IM. It also elevates torque ripple and triggers slip frequency deviations. These effects destabilize motor torque and speed (Mirdas et al., 2023). Increased harmonic content raises current THD. This impacts drive efficiency and motor thermal loading.

displays the impact of m_i, ranging from 0.2 to 2, on motor characteristics. The value of m_i are expressed in Eq. (1) previously. The phase voltage, line voltage, and current have been shown in Figure 8. Figure 8 shows the increase in the ripples and noise in the current due to the high THD value at lower m_i. Furthermore, the current value has increased by increasing the m_i as shown in Figure 8. However, the motor speed has many changes due to increasing the m_i. First, the speed value has increased from 270 rpm to 1400 rpm by increasing the m_i from 0.2 to 2 as shown in Figure 9. Second, the ripple has been increased by raising the m_i value. Lastly, the time needed to reach the steady state speed is decreased significantly from 0.6 to 0.08 sec, as shown in Figure 9.

Table 5: Performance Metrics of Fan Induction Motor with Varying Modulation Index

mi	V_a	I_a	P_{in}	N	P_out	λ	Losses	THD(Ia)
0.2	22	4	279	288	30.6	10.9	249	22
0.4	54	9	1211	637	327.5	27	884	29.3
0.6	106	10.5	3127	1145	1885	60.2	1242	44
0.8	174	9.3	3685	1306	2833	76.4	851	40.7
1	209	9.4	4147	1341	3172	76.4	974	29
1.2	228	16.4	8261	1069	2591	31.3	5670	29.3
1.4	236	15.5	5374	1346	3285	61	2090	39.9
1.6	242	12.8	4615	1406	3577	77.5	1039	50
1.8	247.7	9.4	4462	1362	3471	77.7	991	60
2	250	10.3	5512	1300	3319	60.2	2193	57

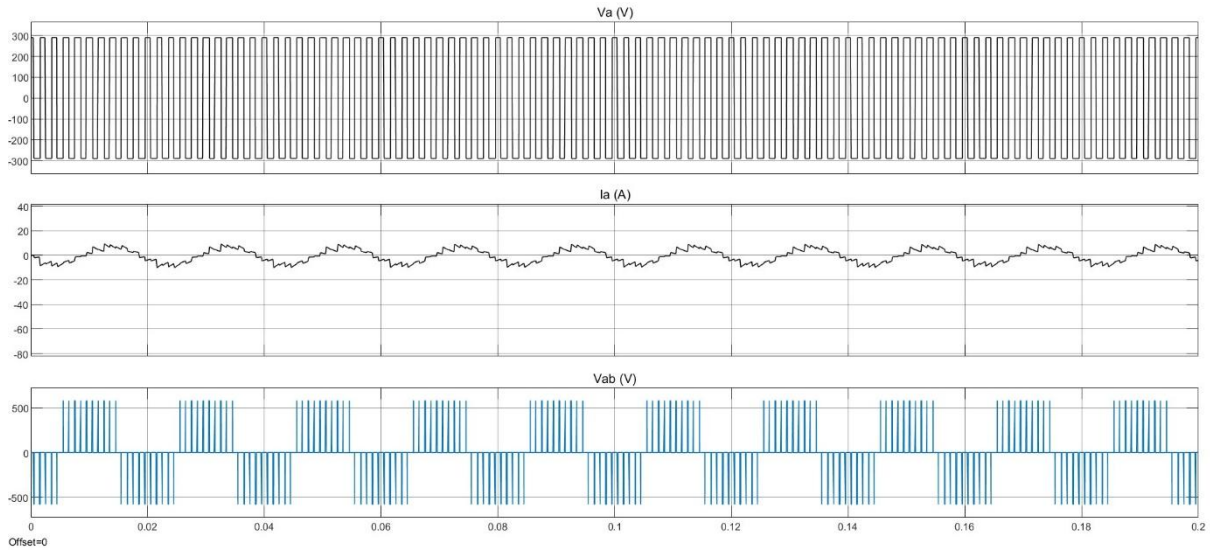

(a)

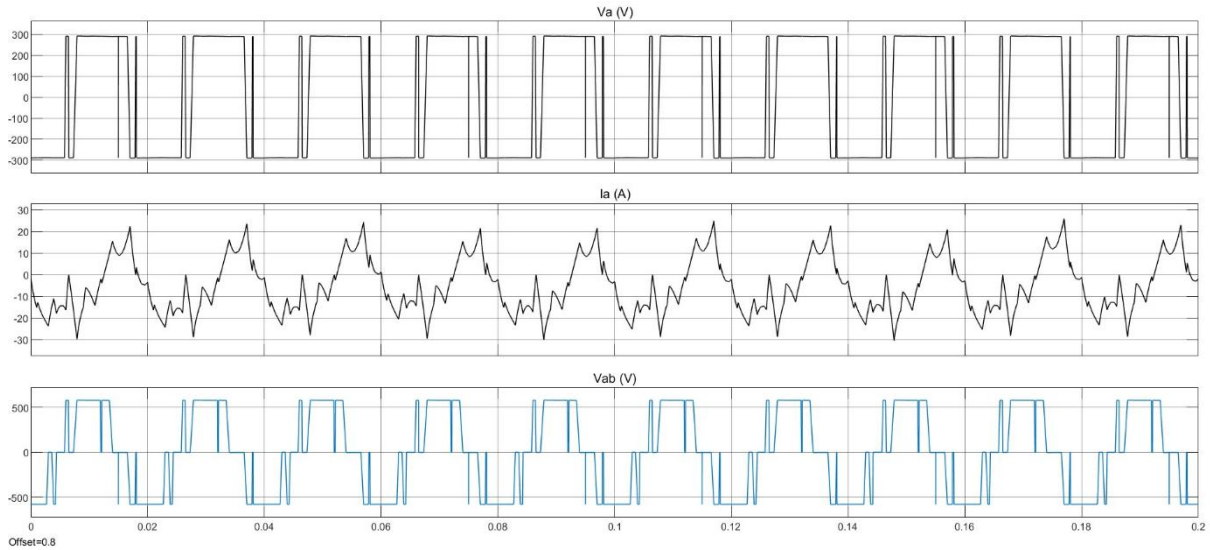

(b)

Figure 8: The line voltage, phase current and phase voltage of modulation index equal to 0.2 (a) and 2 (b)

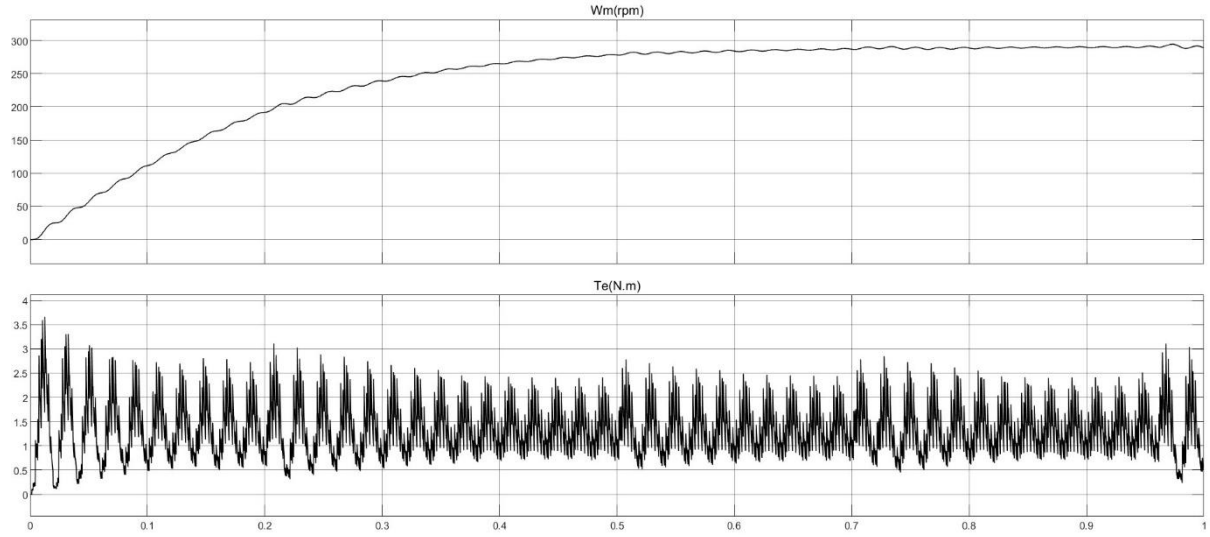

(a)

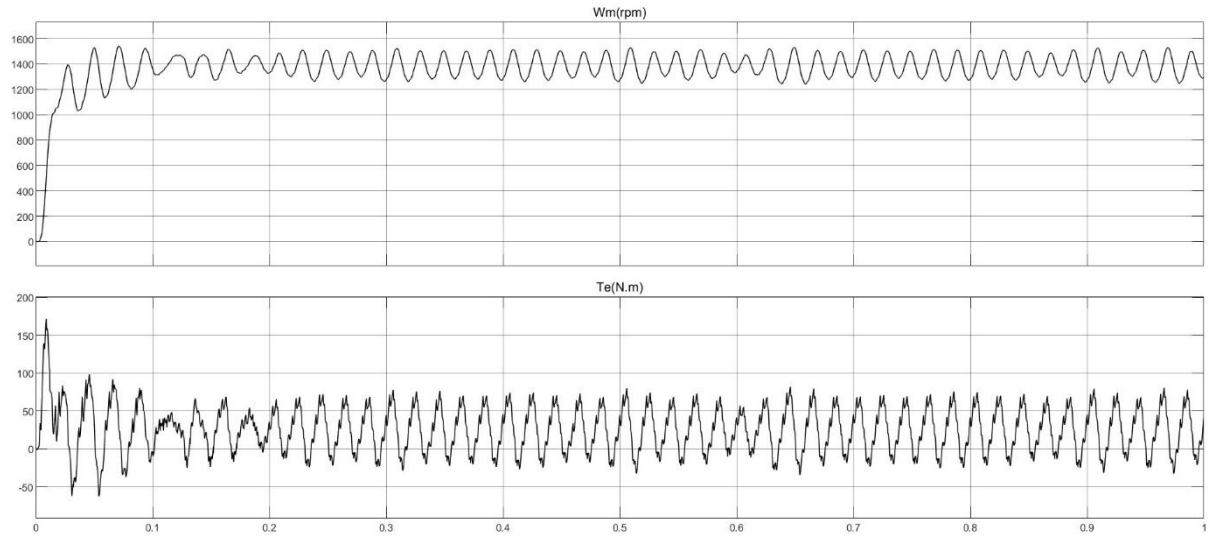

(b)

Figure 9: Motor speed and Torque for modulation index equal to 0.2 (a) and 2 (b)

shows that when m_i exceed 0.8, nonlinearity performance surfaces. For instance, at m_i = 1.2. Despite an increase in input power to 8,261 W, the speed decreases to 1,069 rpm, and efficiency to 31.3%, while THD remains high at 29.3%. This high THD leads to distortion effects, disrupting torque generation and electromagnetic stability. At $m\_i = 1.8$ and 2, THD further escalates beyond 57%. However, output power varies between 3,300 W and 3,570 W, and efficiency varies between 60 and 78%, which are signs of harmonic-induced torque ripple changes. These results confirm the drawback of overmodulation in SPWM , leading to waveform clipping and harmonics that reduce efficiency (IbraheemAbood & Sabri A. Raheem, 2014; Raghuwanshi et al., 2017). This nonlinear behavior stems from SPWM's inherent limitation. The linear modulation index maxes out near 0.785 (π/4). Beyond this, voltage waveforms clip and generate substantial harmonics. The distorted waveform increases copper and iron losses in the IM. It also elevates torque ripple and triggers slip frequency deviations. These effects destabilize motor torque and speed (Mirdas et al., 2023). Increased harmonic content raises current THD. This impacts drive efficiency and motor thermal loading.

3.3 Regular Vs Fan Vs Pump Loads: Motor Performance

Industrial loads vary widely in their torque–speed characteristics. These differences significantly influence motor performance. Regular industrial loads (e.g. conveyors) typically exhibit constant torque that remains independent of motor speed. On the other hand, fan and pump loads have torque proportional to the speed, arising from aerodynamic and hydraulic resistance. Consequently, the torque demand reduces at lower speeds but increases torque and losses as speed rises, as shown previously in Eq. (5), Eq. (8).

Pump loads fall below these two cases, with torque proportional to speed squared, similar to fan loads but shaped by fluid dynamics and hydraulic resistances, as shown in Eq. (8). This is reflected in lower current draw (7.06 A) and input power (1960 W) compared to the regular (9.15 A, 3931 W) and fan loads (9.2 A, 3976 W) for similar motor voltage. It is demonstrating the reduced mechanical load effect at given speeds (Table 6). This reduction aligns with the affinity laws governing pump and fan loads (Eq. (8)), resulting in energy savings at lower speeds (Kazakbaev et al., 2019). Additionally, output power and efficiency are lower for the pump load (1498 W, 76.4%) than the regular load (3190 W, 81.2%) and fan load (3177 W, 79.9%). It reflects inherent hydraulic and core losses within pumps due to a high THD level in the pump current (Goman et al., 2019). In comparison to normal and fan loads, the motor speed under pump load is marginally higher (1,437 rpm vs. 1,366 rpm), which means less electromagnetic torque is required to overcome resistance (Table 6).

In summary, the results verify established understanding of motor-load interactions. The results show that constant torque loads require robust torque delivery at all speeds. Fans and pumps follow torque-speed squared laws, leading to lower efficiency and losses at reduced speeds. These differences underline the importance of tailored motor and drive selection to match load types for improved energy efficiency

Table 6: Regula, Fan, and Pump loads test result

Parameters	Regular Load	Fan Load	Pump Load
$\boldsymbol{V_a(V)}$	206.2	205.9	206
$\boldsymbol{I_a(A)}$	9.15	9.2	7.06
$\boldsymbol{N(rpm)}$	1366	1365	1437
$\boldsymbol{P_{in}(W)}$	3931	3976	1960
$\boldsymbol{P_{out}(W)}$	3190	3177	1498
$\boldsymbol{\lambda(\%)}$	81.16	79.9	76.41
$\boldsymbol{p_l(W)}$	740.4	799.1	462.4
THD(Ia)(%)	9.83	9.49	11

4 Conclusion

This study analyzes induction motor performance under varying modulation indices, carrier frequencies, and load types. These factors affect efficiency and harmonic distortion. Higher f_c reduces harmonic distortion and losses while enhancing waveform smoothness and energy efficiency. Similarly, the input power exhibits non-linear behavior. Peak efficiency (λ = 80%) occurs at $P = 100$, with minimal losses and distortion (THD(I_a) = 3%, which gives a new insight into the FIM performance. Furthermore, the analysis of varying modulation indices (m_i) revealed that $m_i = 0.8$ is the threshold between linear and non-linear relationships between m_i and key motor parameters. For m_i. For example, efficiency rises at m_i = 0.4 and $m\_i = 0.8$ from 27 to 76.4, respectively. While at overmodulation, when m_i As the number increases from 1.6 to 2, the efficiency decreases from 77.5 to 60.2. Beyond this, increased harmonics and losses reduce performance, emphasizing the need for optimized modulation ranges. On the other hand, industrial load types also have different behaviors between the fan, pump, and regular loads. Regular loads show slightly higher efficiency than fan and pump loads because of aerodynamic, hydraulic, and frictional effects. In contrast, the THD value is lowest when the fan load is considered. These findings provide design guidelines for controlling switching parameters to minimize losses,

improve efficiency, and performance. Results are simulation-based only. However, hardware validation and thermal effects require experimental verification as future work, same as the method presented in Ref (Al-Saegh et al., 2024).

Acknowledgements

I sincerely thank my faculty and staff of Department of Electrical and Electronic engineering/ Thi Qar University for their support and resources, as well as to my colleagues for their insightful discussions specially, Dr. Ali Kareem. Finally, I am deeply grateful to my family and friends for their unwavering encouragement and support.

Authorships Contributions

The first author conducted all aspects of the research, including study conception and design, data collection, analysis, interpretation of the results, and manuscript preparation. The second and the third authors supervised the research process and provided scientific guidance and critical revision of the manuscript. All authors reviewed and approved the final version of the manuscript.

Funding Sources

No external funding support was received for this study.

Data Availability

The data that support this study are available from the corresponding author upon request

Conflict of Interest

The authors declare that there are no conflicts of interest regarding the publication of this manuscript

References

Al-Adwan, I. M., & Al Shiboul, Y. A. (2020). Effect of the Modulation Index and the Carrier Frequency on the Output Vol Tage Waveform of the Spwm Voltage Source Inverter. *2020 17th International Multi-Conference on Systems, Signals & Devices (SSD)*, 960–968. https://doi.org/10.1109/SSD49366.2020.9364104

Al-Saegh, A., Daood, A., & Ismail, M. H. (2024). Dual Optimization of Deep CNN for Motor Imagery EEG Tasks Classification. *17(4), 75-91*, *17*(4), 75–91. https://doi.org/10.24237/djes.2024.17405

Ali, S., Khalid, K., Abdul-Hassan, M., & Ali, R. S. (2016). Modeling of Structural Human Dynamic Simulation of Speed Control for Synchronous Reluctance Motor Based on Tuning Cascaded PID Controller with PSO Algorithm. *University of Thi-Qar Journal for Engineering Sciences*, *7*(2 SE-Articles), 1–15. https://doi.org/10.31663/UTJES.V7I2.58

Almani, M. N., Hussain, G. A., & Zaher, A. A. (2021). An Improved Technique for Energy-Efficient Starting and Operating Control of Single Phase Induction Motors. *IEEE Access*, *9*, 12446–12462. https://doi.org/10.1109/ACCESS.2021.3050920

Amin, B. (2001). *Induction Motors*. https://doi.org/10.1007/978-3-662-04373-8

Asif, M. J., Shahbaz, T., Hassan, S. U., & Rizvi, S. T. H. (2016). Mathematical modelling of 3-phase induction motor to study the Torque vs. Speed characteristics using MATLAB Simulink. *2016 19th International Multi-Topic Conference (INMIC)*, 1–7. https://doi.org/10.1109/INMIC.2016.7840144

Asker, M. E., & Kilic, H. (2017). Modulation Index And Switching Frequency Effect On Symmetric Regular Sampled SPWM. *European Journal of Technic*, *7*(2), 102–109. https://doi.org/10.23884/ejt.2017.7.2.04

Birowo, B., Ahmad, R., Zamzuri, H., & Priyono, A. (2015). Vector controlled comparative studies for line starting performance induction motor of a conveyor system. In *Recent Advances in Electrical Engineering Series | 47* (pp. 153–158). WSEAS Press.

Busacca, A., Di Tommaso, A. O., Miceli, R., Nevoloso, C., Schettino, G., Scaglione, G., Viola, F., & Colak, I. (2022). Switching Frequency Effects on the Efficiency and Harmonic Distortion in a Three-Phase Five-Level CHBMI Prototype with Multicarrier PWM Schemes: Experimental Analysis. *Energies*, *15*(2), 586. https://doi.org/10.3390/en15020586

Dems, M., & Komeza, K. (2022). Designing an Energy-Saving Induction Motor Operating in a Wide Frequency Range. *IEEE Transactions on Industrial Electronics*, *69*(5), 4387–4397. https://doi.org/10.1109/TIE.2021.3082057

Diyoke, G. C., Eya, C. U., Obi, P. I., & Onwuka, I. K. (2024). Performance Analysis of Inverter Fed Single Phase Induction Motor Drive. *ABUAD Journal of Engineering Research and Development (AJERD)*, *7*(1), 231–240. https://doi.org/10.53982/ajerd.2024.0701.24-j

FFT Analyzer. (n.d.). Retrieved December 30, 2024, from https://www.mathworks.com/help/sps/powersys/ref/fftanalyzer-app.html

Goman, V., Oshurbekov, S., Kazakbaev, V., Prakht, V., & Dmitrievskii, V. (2019). Energy Efficiency Analysis of Fixed-Speed Pump Drives with Various Types of Motors. *Applied Sciences 2019, Vol. 9, Page 5295*, *9*(24), 5295. https://doi.org/10.3390/APP9245295

Guo, X., Wu, Y., Li, G., & Lu, C. (2017). Dynamic simulation of an induction-motor centrifugal-pump system under variable speed conditions. *Elektrotehniski Vestnik/Electrotechnical Review*, *84*(3), 125–132. https://ev.fe.uni-lj.si/3-2017/Xiwen.pdf

Hassain, R. H., Kadhim, A., Aubbas, A., & Man'aa Dakil, A. (2018). Independent Control of a Dual Induction Motors Drives Control Based on Indirect Field Vector Oriented Method. *University of Thi-Qar Journal for Engineering Sciences*, *9*(1), 64–72. https://doi.org/10.31663/UTJES.V9I1.46

IbraheemAbood, S., & Sabri A. Raheem, M. (2014). Performance Analysis of SPWM and SVPWM Inverters Fed Induction Motor. *International Journal of Computer Applications*, *86*(5), 33–38. https://doi.org/10.5120/14984-3191

Infineon Technologies AG. (2013). *High speed switching series fifth generation: IKW40N65F5*. https://www.infineon.com/dgdl/Infineon-IKW40N65F5-DS-v01_02-EN.pdf?fileId=db3a30433af5291e013afa60c5395f31#page=2.00

Jung, H. S., Hwang, C. E., Kim, H. S., Sul, S. K., Hee Won, A., & Yoo, H. (2018). Minimum Torque Ripple Pulse Width Modulation With Reduced Switching Frequency for Medium-Voltage Motor Drive. *IEEE Transactions on Industry Applications*, *54*(4), 3315–3325. https://doi.org/10.1109/TIA.2018.2808480

Kazakbaev, V., Prakht, V., Dmitrievskii, V., Ibrahim, M. N., Oshurbekov, S., & Sarapulov, S. (2019). Efficiency Analysis of Low Electric Power Drives Employing Induction and Synchronous Reluctance Motors in Pump Applications. *Energies 2019, Vol. 12, Page 1144*, *12*(6), 1144. https://doi.org/10.3390/EN12061144

Klimenta, D., Hannukainen, A., & Arkkio, A. (2018). Estimating the parameters of induction motors in different operating regimes from a set of data containing the rotor cage temperature. *Electrical Engineering*, *100*(1), 139–150. https://doi.org/10.1007/s00202-016-0497-8

Krings, A., Soulard, J., & Wallmark, O. (2013). Influence of PWM Switching Frequency and Modulation Index on The Iron Losses and Performance of Slot-Less Permanent Magnet Motors. *2013 International Conference on Electrical Machines and Systems (ICEMS)*, 474–479. https://doi.org/10.1109/ICEMS.2013.6713113

Lai, Y. S., & Chen, J. H. (2001). A new approach to direct torque control of induction motor drives for constant inverter switching frequency and torque ripple reduction. *IEEE Transactions on Energy Conversion*, *16*(3), 220–227. https://doi.org/10.1109/60.937200

Marino, R., Tomei, P., & Verrelli, C. M. (2010). *Induction Motor Control Design*. *0*. https://doi.org/10.1007/978-1-84996-284-1

Mirdas, Q. H., Yasin, N. M., & Alshamaa, N. K. (2023). Analytical comparison of SPWM & SVPWM techniques for three-phase induction motor V/F speed control. *AIP Conference Proceedings*, *2804*(1). https://doi.org/10.1063/5.0154520

Mohammed, Z. R., & Hadi, A. R. S. (2024). Torque Ripple Rate Reduction Of 6/4 Switched Reluctance Motor Using Sliding Mode Learning Controls. *Kufa Journal of Engineering*, *15*(4), 18–33. https://doi.org/10.30572/2018/KJE/150402

Nandi, S., Toliyat, H. A., & Li, X. (2005). Condition Monitoring and Fault Diagnosis of Electrical Motors—A Review. *IEEE Transactions on Energy Conversion*, *20*(4), 719–729. https://doi.org/10.1109/TEC.2005.847955

Nasir, B. A. (2022). Determination of the Harmonic Losses in an Induction Motor Fed by an Inverter. *Engineering, Technology & Applied Science Research*, *12*(6), 9536–9545. https://doi.org/10.48084/ETASR.5012

Rachev, S., & Dimitrov, L. (2022). Evaluation of the behaviour of an induction motor for fan system under various external factors. *IOP Conference Series: Materials Science and Engineering*, *1216*(1), 012007. https://doi.org/10.1088/1757-899X/1216/1/012007

Raghuwanshi, S. S., Khare, V., & Gupta, K. (2017). Analysis of SPWM VSI fed AC drive using different modulation index. *2017 International Conference on Information, Communication, Instrumentation and Control (ICICIC)*, *2018-Janua*, 1–6. https://doi.org/10.1109/ICOMICON.2017.8279070

Rahman, K., Rahman, S., Samiullah, M., Iqbal, A., & Ashraf, I. (2019). V/f Control of Five-Phase Induction Motor Drive Fed from Cascaded H Bridge Multilevel Inverter. *Proceedings - 2019 International Conference on Electrical, Electronics and Computer Engineering, UPCON 2019*. https://doi.org/10.1109/UPCON47278.2019.8980274

Sarigiannidis, A. G., & Kladas, A. G. (2015). Switching Frequency Impact on Permanent Magnet Motors Drive System for Electric Actuation Applications. *IEEE Transactions on Magnetics*, *51*(3), 1–4. https://doi.org/10.1109/TMAG.2014.2358378

Sharma, A., N., A., & Gao, S. (2020). Modulation index effect on inverter based induction motor drive. *International Journal of Power Electronics and Drive Systems (IJPEDS)*, *11*(4), 1785. https://doi.org/10.11591/ijpeds.v11.i4.pp1785-1798

Solangi, A. A., Gul, M., Shaikh, R., Umer, F., Khan, N., & Anjum, Z. (2018). Effects of Modulation Index on Harmonics of SP-PWM Inverter Supplying Universal Motor. *International Journal of Advanced Computer Science and Applications*, *9*(7), 167–174. https://doi.org/10.14569/IJACSA.2018.090724

Thomson, W. T., & Culbert, I. (2016). Current Signature Analysis for Condition Monitoring of Cage Induction Motors: Industrial Application and Case Histories. *Current Signature Analysis for Condition Monitoring of Cage Induction Motors: Industrial Application and Case Histories*, 1–397. https://doi.org/10.1002/9781119175476